(*N*,*N*-Dimethylaminoxy)trifluorosilane: Strong, Dipole Moment Driven Changes in the Molecular Geometry Studied by Experiment and Theory in Solid, Gas, and Solution Phases

Norbert W. Mitzel,*,† Udo Losehand,† Anan Wu,‡ Dieter Cremer,*,‡ and David W. H. Rankin§

Contribution from the Anorganisch-chemisches Institut der Technischen Universität München, Lichtenbergstrasse 4, 85747 Garching, Germany, Department of Theoretical Chemistry, Göteborg University, Reutersgatan 2, S-41320 Göteborg, Sweden, and Department of Chemistry, University of Edinburgh, West Mains Road, Edinburgh EH9 3JJ, U.K.

Received December 30, 1999

Abstract: (*N*,*N*-Dimethylaminoxy)trifluorosilane, $F_3SiONMe_2$ (**1**), was prepared by the reaction of $LiONMe_2$ with SiF_4 in Me_2O at −96 °C as a colorless, air-sensitive liquid, which was identified by gas-phase IR spectroscopy and NMR spectroscopy of the nuclei ^1H, ^{13}C, ^{15}N, ^{17}O, ^{19}F, and ^{29}Si. The gas-phase geometry of **1**, as determined by electron diffraction analysis refined in C_s symmetry, is influenced by weak attractive interactions between Si and N: Si···N 2.273(17) Å, Si−O−N 94.3(9)°, [Si−O 1.619(8) Å, N−O 1.479(7) Å, O−Si−$F_{in-plane}$ 104.1(10)°, O−Si−$F_{out-of-plane}$ 111.8(10)°]. X-ray diffraction analysis of **1** reveals that intramolecular Si···N interactions are much stronger in the solid state than in the gas phase: Si···N 1.963(1) Å, Si−O−N 77.1(1)° [Si−O 1.639(1) Å, N−O 1.508(1) Å, O−Si−$F_{in-plane}$ 102.5(1)°, O−Si−$F_{out-of-plane}$ 118.0(1)° and 120.1(1)°]. Using measured NMR chemical shifts in C_6D_6 solution, the geometry of **1** in solution was determined with the NMR/ab initio/DFT-IGLO method to fall between that of the gas-phase geometry and the geometry in the solid state. MP2 and DFT calculations reveal that electrostatic interactions between **1** and the surrounding medium increase with the dielectric constant ϵ since mutual charge polarization enhances the molecular dipole moment from 4 to more than 6 D, which implies a compression of the Si−O−N angle and the Si···N distance. Since electrostatic attraction between N and Si supports these changes, the increase in molecular energy upon reduction of the Si···N distance is small and compensated by the gain of stabilizing intermolecular interactions. The analysis of the calculated electron density distribution shows that the main aspects of bonding in **1** are not changed in the solid state and that the Si···N attraction is not of covalent nature, but rather due to strong electrostatic and dipole interactions.

1. Introduction

It is generally assumed that molecular structures do not differ much between the gas phase, solution, or solid state provided there are no significant chemical interactions between the target system and its environment. However, spectacular exceptions from this rule exist in those cases where molecules are easily deformed, e.g. by electrostatic interactions with the environment. Recent reviews by Leopold and co-workers[1] describe donor−acceptor (D−A) complexes, in which the interaction distance between D and A can change by more than 30% when the system is transferred from the gas phase to the solid state. Typical examples are amine−borane[1] and amine−alane adducts,[2] which undergo dramatic contraction of their B−N and Al−N bonds caused by an increase of the molecular dipole moment upon changing from the gas phase to the highly polar surrounding in the crystal lattice.[1]

While most of these examples can be classified as intermolecular D−A complexes (at least formally they result from interactions between a D and an A molecule),[3] there are molecules that change their structure depending on the environment because of *intramolecular* D−A interactions. Examples comprise various silatranes[4] and compounds extensively investigated by Corriu[5] and others, in which D−A interactions between Si and one (or more) N atom(s) separated by several bonds are responsible for the structural changes, which depend on the surrounding medium.[6] An even more spectacular structural change is observed when the D and A atoms are separated by just two classical covalent bonds. Mitzel and Losehand[7] investigated compounds with D ($-NR_2$) and A

† Technische Universität München.

‡ Göteborg University.

§ University of Edinburgh.

(1) (a) Leopold, K. R.; Canagaratna, M.; Phillips, J. A. *Acc. Chem. Res.* **1997**, *30*, 57. (b) Leopold, K. R. In *Advances in Molecular Structure Research*; Hargittai, M., Hargittai, I., Eds.; JAI Press: Greenwich, CT, 1996; Vol. 2, p 103.

(2) Müller, J.; Ruschewitz, U.; Indris, O.; Hartwig, H.; Stahl, W. *J. Am. Chem. Soc.* **1999**, *121*, 4647.

(3) Haaland, A. *Angew. Chem., Int. Ed. Engl.* **1989**, *28*, 992.

(4) (a) Forgacs, G.; Kolonits, M.; Hargittai, I. *Struct. Chem.* **1990**, *1*, 245. (b) Parkanyi, L.; Hencsei, P.; Bihatsi, L.; Müller, T. *J. Organomet. Chem.* **1984**, *269*, 1. (c) Shen, Q.; Hilderbrandt, R. L. *J. Mol. Struct.* **1980**, *64*, 257. (d) Parkanyi, L.; Bihatsi, L.; Hencsei, P. *Cryst. Struct. Commun.* **1978**, *7*, 435.

(5) (a) Chuit, C.; Corriu, R. J. P.; Mehdi, A.; Reyé, C. *Angew. Chem.* **1993**, *105*, 1372. (b) Carré, F.; Chuit, C.; Corriu, R. J. P.; Mehdi, A.; Mehdi, A. *Angew. Chem., Int. Ed. Engl.* **1994**, *33*, 1097. (c) Chauhan, M.; Chuit, C.; Corriu, R. J. P.; Reyé, C. *Tetrahedron Lett.* **1996**, *37*, 845.

(6) For a recent review, see: Ottosson, C.-H.; Kraka, E.; Cremer D. In *Pauling's Legacy: Modern Modelling of the Chemical Bond*; Maksic, Z. B., Orville-Thomas, W. J., Eds.; Theoretical and Computational Chemistry, Vol. 6; Elsevier: Amsterdam, 1999; p 231.

10.1021/ja994542w CCC: $19.00
Published on Web 04/21/2000

(−SiX_3) groups in geminal positions to one another, thus potentially being capable of changing from an acyclic $X_3Si-O-NR_2$ molecule to potential three-membered-ring structures with the possibility of a weak Si−N bond produced by increased D−A interactions.

Such systems were also described for various combinations of p-block-elements including B−C−N,[8] B−N−N,[9] Al−C−N,[10] Al−N−N,[11] Si−N−N,[12] Ge−O−N,[13] and Sn−O−N.[14] For the Si−O−N unit contained in aminoxysilanes and oximatosilanes, it was found that the strength of the attractive interactions between Si and N atoms depends on the nature of the substituents at Si and N and the orientation of the most electronegative Si substituent relative to the SiON plane.[7] Simple electrostatic attraction between positively charged Si and negatively charged N centers seemed to be insufficient to account for the details of the observed molecular structures, which show large variations in Si−O−N angles and Si−N distances, e.g. $MesF_2SiON(SiMe_3)_2$ [2.696 Å, 117.7(1)° solid],[15] $Me_3SiON(CF_3)_2$ [2.66 Å, 113.4(19)° gas],[16] $Me_3SiONMe_2$ [2.566(8) Å, 107.9(6)° gas],[17] $H_3SiONMe_2$ [2.453(1) Å, 102.6(1)° solid],[7] $Cl_3SiONMe_2$ [2.437(av) Å, 103.0(av)° solid],[18] $H_2Si(ONMe_2)_2$ [2.138(av) Å, 95.2(av)° solid],[19] and $ClH_2SiONMe_2$ [anti conformer in the solid state 2.028(1) Å, 79.7(1)°].[20] It is the general understanding that for the latter compounds with small Si−O−N angles a weak bond is established. However, so far there are no other than structural data to confirm this assumption.

In this work, we present a detailed spectroscopic, structural, and quantum chemical study of (*N*,*N*-dimethylaminoxy)trifluorosilane, $F_3SiONMe_2$ (**1**), which exhibits the strongest Si−N attraction found for aminoxysilanes so far. We use the analysis of X-ray-diffraction and electron-diffraction data to determine the structure of **1** both in the solid state and in the gas phase. In addition, solution NMR spectroscopy in combination with the NMR/ab initio/IGLO method[21] describe the structure of **1** dissolved in benzene. Utilizing the results of quantum chemical calculations, in particular carried out with second-order Møller−Plesset perturbation theory (MP2)[22] and density functional theory (DFT),[23] we analyze and explain structural changes of **1** depending on the surrounding media. In particular, we focus on the question, whether a chemical bond is established between Si and N in condensed phases utilizing the calculated electron density distribution and criteria developed for covalent bonding.[24]

2. Results

In this section we discuss the synthesis of $F_3SiONMe_2$ (**1**), its spectroscopic characterization, the experimental determination of its structure in the solid state and the gas phase, and its structure in solution determined by the NMR/ab initio/IGLO method.

Synthesis and Characterization. The preparation of **1** is preferentially carried out by reaction of lithiated *N*,*N*-dimethylhydroxylamine, $LiONMe_2$, with SiF_4 in dimethyl ether at −96 °C. Fluorination of $Cl_3SiONMe_2$[18] with lead difluoride or tributyltin fluoride was found to be not a suitable route for the preparation of **1**, as these reactions remain always incomplete and lead to mixtures of chlorinated/fluorinated aminoxysilanes in low yields. Compound **1** is separated by fractional condensation from the remaining SiF_4 and the low-boiling, more volatile solvent. The SiF_4 employed in this reaction was generated from $SiCl_4$ with SbF_3 in diethyl ether.

$$3SiCl_4 + 4SbF_3 \rightarrow 3SiF_4 + 4SbCl_3$$

$$SiF_4 + LiONMe_2 \rightarrow F_3SiONMe_2 + LiF$$

Compound **1** is a colorless extremely air-sensitive liquid that etches glass surfaces in the presence of traces of moisture. The identity and purity of $F_3SiONMe_2$ were proven by gas-phase IR spectroscopy and NMR spectroscopy of the six nuclei ^1H, ^{13}C, ^{15}N, ^{17}O, ^{19}F, and ^{29}Si in C_6D_6 solution. Attempts to record a mass spectrum failed.

The proton NMR spectrum shows one signal at 2.11 ppm, which is at relatively low frequency for $SiONMe_2$ linkages. The signal is split into a quartet (J_{FH} = 0.7 Hz) by coupling with the three ^{19}F nuclei. Coupling to the ^{19}F nuclei atoms is also observed in the ^{15}N NMR spectrum, which exhibits a quartet at −249.2 ppm. While the ^{15}N NMR chemical shift of **1** does not follow the trend of increasing deshielding with increasing electronegativity of the substituents at the Si atom as observed in the series $Me_3SiONMe_2$ (−247.8 ppm), $H_3SiONMe_2$ (−234.0 ppm), and $Cl_3SiONMe_2$ (−229.4 ppm), its value is similar to that of $ClH_2SiONMe_2$ (−249.2 ppm). The J_{FN} coupling constant is −9.3 Hz, which is relatively large and probably indicates Si···N interactions in the benzene solution. The high electron-withdrawing potential of the fluorine atoms shifts the ^{29}Si NMR signal (quartet) to low frequencies (−117.2 ppm). The ^{19}F NMR spectrum contains a single singlet at −162.0 ppm, i.e., the $^5J_{FH}$ coupling was not resolved.

Crystal Structure. Utilizing in situ techniques a single crystal of **1** was grown at its melting point of −64 °C and an X-ray diffraction experiment was performed. In the crystal lattice ($P2_1/n$), the molecules form isolated units without crystallographic symmetry, but approximate molecular C_s symmetry (Figure 1). Geometric parameters are listed in Table 1.

Most striking in the crystal structure is the short Si···N distance of 1.963(1) Å, which is close to the sum of the covalent radii of Si and N (1.80−1.92 Å), but about 0.2 Å longer than

(7) Mitzel, N. W.; Losehand, U. *Angew. Chem., Int. Ed. Engl.* **1997**, *36*, 2807.
(8) Brauer, D. J.; Bürger, H.; Buchheim-Spiegel, S.; Pawelke, G. *Eur. J. Inorg. Chem.* **1999**, 255.
(9) Diemer, S.; Nöth, H.; Storch, W. *Eur. J. Inorg. Chem.* **1999**, 1765.
(10) Uhl, W.; Schütz, U.; Hiller, W.; Heckel, M. *Chem. Ber.* **1994**, *127*, 1587.
(11) Uhl, W.; Hannemann, F. *Eur. J. Inorg. Chem.* **1999**, 201.
(12) Mitzel, N. W. *Chem. Eur. J.* **1998**, *4*, 692.
(13) Losehand, U.; Mitzel, N. W. *Eur. J. Inorg. Chem.* **1998**, 2023.
(14) Mitzel, N. W.; Losehand, U.; Richardson, A. *Organometallics* **1999**, *18*, 2610.
(15) Wolfgramm, R.; Klingebiel, U.; Noltemeyer, M. *Z. Anorg. Allg. Chem.* **1998**, *624*, 856.
(16) Hertel, T.; Jakob, J.; Minkwitz, R.; Oberhammer, H. *Inorg. Chem.* **1998**, *37*, 5092.
(17) Mitzel, N. W.; Losehand, U.; Richardson, A. D. *Inorg. Chem.* **1999**, *38*, 5323.
(18) Mitzel, N. W.; Losehand, U.; Rankin, D. W. H. *J. Chem. Soc., Dalton Trans.* **1999,** 4291.
(19) Losehand, U.; Mitzel, N. W. *Inorg. Chem.* **1998**, *37*, 3175.
(20) Mitzel, N. W.; Losehand, U. *J. Am. Chem. Soc.* **1998**, *120*, 7320.
(21) For a description of the NMR/ab initio/IGLO method see, e.g.: (a) Reference 5. (b) Cremer, D.; Olsson, L.; Reichel, F.; Kraka, E. *Isr. J. Chem.* **1993**, *33*, 369.
(22) For a recent review,see: Cremer, D. In *Encyclopedia of Computational Chemistry*; Schleyer, P. v. R., Allinger, N. L., Clark, T., Gasteiger, J., Kollman, P. A., Schaefer, H. F., Schreiner, P. R., Eds.; John Wiley: Chichester, UK, 1998; Vol. 3, p 1706.
(23) (a) Hohenberg, P.; Kohn, W. *Phys. Rev.* **1994**, *136*, B864. (b) Kohn, W.; Sham, L. *J. Phys. Rev.* **1965**, *140*, A1133.
(24) Kraka, E.; Cremer, D. In *Theoretical Models of the Chemical Bond, Part 2: The Concept of the Chemical Bond*; Maksic, Z. B., Ed.; Springer: New York, 1990; p 453.

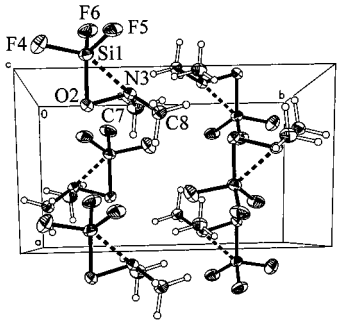

Figure 1. Solid-state structure of $F_3SiONMe_2$ (**1**) as determined by low-temperature X-ray crystallography. The contents of the unit cell are shown at the 40% probability level.

Table 1. Solid-State and Gas-Phase Geometries for **1**[a]

	solid state			gas phase		
	XRD	MP2	B3LYP	GED	MP2	B3LYP
Si−O	1.639(1)	1.674	1.664	1.618(8)	1.643	1.626
O−N	1.508(1)	1.492	1.495	1.478(7)	1.476	1.478
Si···N	1.963(1)	1.976	1.971	2.273(17)	2.286	2.439
Si−F4	1.585(1)	1.601	1.597	1.566(4)	1.590	1.578
Si−F5/6	1.577/ 1.574(1)	1.600	1.592	1.564(2)	1.589	1.580
N−C7/8	1.461/ 1.453(1)	1.461	1.462	1.453(4)	1.458	1.456
SiON	77.1(1)	77.1 fixed	77.1 fixed	94.3(9)	94.1	103.5
OSiF4	102.5(1)	103.0	102.6	104.1(10)	106.1	106.8
OSiF5/6	118.0/ 120.1(1)	117.3	117.8	111.8(10)	113.9	113.2
ONC7/8	108.5/ 107.5(1)	107.8	108.3	107.0(6)	105.7	105.8
Pyr(Si)	47.8(1)	43.8	44.6	31.6(15)	37.5	36.7
Pyr(N)	31.4(1)	31.3	30.2	31.9(12)	36.3	35.6

[a] Determined by low-temperature X-ray crystallography (XRD) and gas electron-diffraction (GED) using the SARACEN method with MP2/6-311G(d,p) restraints (see Table 2). For comparison with the crystallographic results geometry parameters were calculated at MP2/6-311G(d,p) and B3LYP/6-311+G(3df,3pd) levels of theory with the Si−O−N angles fixed at the experimental solid-state values. The calculated gas-phase values at the same levels represent completely optimized geometries. The pyramidalization angles at Si and N are defined by the expression $360 - \sum_{i=1,3}\alpha_i$, where α_i denotes the bending angles at Si and N.

the Si−N distance in typical silylamines (H_3SiNMe_2, 1.724 Å).[25] However, these values refer to tetracoordinate Si atoms, while corresponding values for hypercoordinate silicon can be expected to be larger ($ClH_3Si{\cdot}NH_3$: 2.78 Å).[25]A better reference system is thus the Si−N bond length in silylammonium fragments [$H_3SiNH_3^+$, 1.917 Å;[25] {[$H_2SiN(i\text{Pr})$]$_2$Si(NH*i*Pr)-(NH_2iPr)}CF_3SO_3, 1.825(5) Å[26]]. The short Si−N distance in **1** implies a valence angle at oxygen of only 77.1(1)°, which represents the smallest Si−O−N angle ever found in an aminoxysilane. Only $ClH_2SiONMe_2$ has a comparable strong attraction between Si and N leading to a Si···N distance of 2.028(1) Å and a Si−O−N angle of 79.7(1)°.[20] The Si−O−N angle in the Cl-analogue $Cl_3SiONMe_2$ is as much as 25.9° larger despite the fact that the electronic nature of **1** and $Cl_3SiONMe_2$ should be similar.[18] The N−O bond in $F_3SiONMe_2$ [1.508(1) Å] is the longest found in all aminoxysilanes and there seems to be a correlation between the length of the N−O bond and the strength of the Si···N interaction.

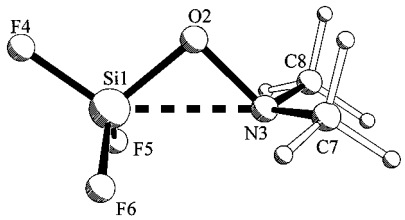

Figure 2. Atom numbering scheme and molecular geometry of $F_3SiONMe_2$ (**1**) as determined by gas-phase electron-diffraction.

The attraction between Si and N atom leads to a pronounced distortion of the coordination geometry at silicon, which is closer to a trigonal bipyramid than to a tetrahedron. The F atoms above and below the SiON plane (F_{oop}) occupy two of the equatorial positions and the in-plane F atom (F_{ip}) one of the axial positions. The O−Si−F_{oop} angles are widened by about 10° with respect to the tetrahedral angle [118.0(1), 120.1(1)°, Figure 1] and are close to the ideal equatorial angle (120°) of a trigonal bipyramid. On the other hand, the O−Si−F_{ip} angle is markedly compressed [102.5(1)°, Figure 1] and the Si−F_{ip} distance is slightly longer [1.585(1) Å, Figure 1] than the Si−F_{oop} bond lengths [1.574-(1),; 1.577(1) Å, Figure 1].

There are no close contacts between molecules **1** in the crystal lattice, i.e., the solid-state molecular structure is influenced just by the dielectric constant ϵ of the crystal lattice rather than steric packing effects. The shortest interatomic distances of interest between the molecules are F···H distances of 2.784 and 2.572 Å and F···F distances of 3.234 and 3.442 Å, respectively. As in the case of $ClH_2SiONMe_2$, the crystal structure does not reveal any significant intermolecular interactions, which suggests that the acceptor properties of the $OSiF_3$ group and the donor capacity of the NMe_2 group are strongly reduced because of intramolecular Si···N interactions.

Gas-Phase Structure. The high volatility of **1** allowed determination of the gas-phase structure by means of analysis of gas-phase electron-diffraction (GED) data. The usual limitations of the GED technique were overcome by application of the SARACEN method,[27] i.e., by supporting the refinement of the experimental scattering intensities by flexible restraints derived from ab initio calculations. The most important geometrical parameters determined in the GED analysis are shown in Figure 2, the geometric parameter values in Table 1, the experimental diffraction data in Figure 3a, and the radial distribution curve in Figure 3b.

The mathematical model for the least-squares refinement of both compounds was defined in C_s symmetry, being based on eight bond lengths, eight angles, and four torsional angles. Definitions of these parameters, the applied restraints, and the final values are listed in Table 2. A total of 20 geometrical parameters were refined under the action of 12 restraints defining the differences of parameters of similar nature or absolute values in the case of hydrogen-defining parameters. Also 21 amplitudes of vibration were refined concurrently under the action of 12 restraints. These amplitudes represent all pairs of scatterers with a contribution exceeding 5% of the Si−F scatterer pair. The amplitude restraints were taken from the MP2/6-31G(d) force field and transformed into amplitudes by means of the program ASYM40[28] after scaling it by an overall factor of 0.93 previously

(25) (a) Olsson, L.; Ottosson, C.-H.; Cremer. D. *J. Am. Chem. Soc.* **1995**, *117*, 7460. (b) Cremer, D.; Olsson, L.; Ottosson, H. *J. Mol. Struct. (THEOCHEM)* **1993**, *33*, 388. (c) Arshadi, M.; Johnels, D.; Edlund, U.; Ottosson, C.-H.; Cremer, D. *J. Am. Chem. Soc.* **1996**, *118*, 5120.

(26) Söldner, M.; Schier, A.; Schmidbaur, H. *Inorg. Chem.* **1998**, *37*, 510.

(27) (a) Blake, A. J.; Brain, P. T.; McNab, H.; Miller, J.; Morrison, C. A.; Parsons, S.; Rankin, D. W. H.; Robertson H. E.; Smart, B. A. *J. Phys. Chem.* **1996**, *100*, 12280. (b) Brain, P. T.; Morrison, C. A.; Parsons, S.; Rankin, D. W. H. *J. Chem. Soc., Dalton Trans.* **1996**, 4589.

(28) Hedberg, L.; Mills, I. M. *ASYM20, ASYM40, Programs for Force Constants and Normal Coordinate Analysis*, Version 3.0, June 1994; see also: Hedberg, L.; Mills, I. M. *J. Mol. Spectrosc.* **1993**, *160*, 117.

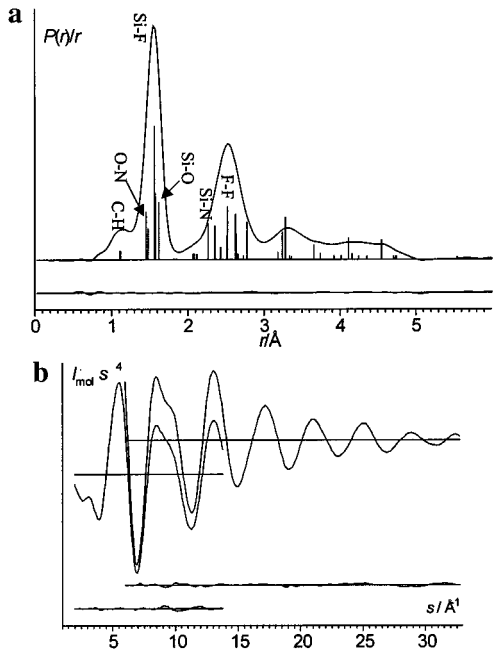

Figure 3. (a) Experimental and difference radial distribution curves for the electron diffraction refinement of $F_3SiONMe_2$. Before Fourier inversion the data were multiplied by $s\cdot\exp[(-0.002s^2)/(Z_{Si} - f_{Si})(Z_F - f_F)]$. Vertical lines indicate atom pairs with their height being proportional to their scattering contribution. (b) Experimental and final difference molecular scattering intensity curves as obtained by electron diffraction of gaseous $F_3SiONMe_2$.

Table 2. Final Geometry Parameter Values and Restraints for the Electron-Diffraction Refinement of Gaseous $F_3SiONMe_2$ and Calculated Values (MP2/6-311G**) for Comparison (in Å and deg)

no.	parameter	GED value	restraint	MP2/6-311G**
p_1	Si−F4	1.566(4)		1.590
p_2	Si−F5/6	1.564(2)	$p_2 - p_1 = -0.001(5)$	1.589
p_3	Si−O	1.618(8)	$p_3 - p_2 = 0.054(10)$	1.643
p_4	O−N	1.478(7)		1.476
p_5	N−C	1.453(4)	$p_5 - p_4 = 0.018(10)$	1.458
p_6	C7−H9	1.108(7)		1.090
p_7	C7−H10	1.111(8)	$p_7 - p_6 = 0.003(5)$	1.093
p_8	C7−H11	1.117(8)	$p_7 - p_6 = 0.008(5)$	1.098
p_9	∠OSiF4	104.1(10)		106.1
p_{10}	∠SiON	94.3(9)		94.1
p_{11}	∠ONC	107.1(6)		105.7
p_{12}	∠C7NC8	114.1(9)	$p_{12} - p_{11} = 6.6(10)$	112.3
p_{13}	∠OSiF5/6	111.8(10)	$p_{13} - p_9 = 7.8(5)$	113.9
p_{14}	∠NC7H9	107.6(8)	$p_{14} = 108.8(10)$	108.8
p_{15}	∠NC7H10	106.0(9)	$p_{14} - p_{15} = 1.5(5)$	107.7
p_{16}	∠NC7H11	109.9(9)	$p_{14} - p_{16} = 2.3(5)$	111.1
p_{17}	τCNCH9	−171.4(59)		−177.9
p_{18}	τCNCH10	71.1(59)	$p_{18} - p_{17} = 241.8(30)$	63.9
p_{19}	τCNCH11	−50.9(61)	$p_{19} - p_{17} = 121.1(30)$	−56.8
p_{20}	τNOSiF5	64.7(4)		63.1

used in connection with the SARACEN method.[29] These amplitudes and restraints are given in Table 3 while Table 4 lists relevant correlation matrix elements. The quality of the refinement can be assessed from the residuals in the molecular scattering curves (Figure 3a) and the radial distribution curves (Figure 3b). Due to the relatively large deviations between the predictions of the SiON angles by MP2/6-311G(d,p) (94.1°) and B3LYP/6-311++G(d,p) calculations (105.5°), an additional refinement with restraints and a start geometry derived from B3LYP/6-311++G(d,p) calculations was undertaken, but converged at a geometry that was almost exactly the same as the reported one. This again bears witness to how important it still is to determine gas-phase structures experimentally. The MP2 method seems thus to be far superior in describing the attractive Si···N interaction.

(29) This scaling factor fits well with the generally accepted scaling factor of 0.9496 for MP2-fc/6-311G(d,p): Scott, A. P.; Radom L. *J. Phys. Chem.* **1996**, *100*, 16502.

Table 3. Selected Interatomic Distances [Å], Amplitudes of Vibration [Å], and Amplitude Restraints for the Electron-Diffraction Refinement of Gaseous $F_3SiONMe_2$

no.	atom pair	distance	amplitude	restraint
d_1	Si1−F4	1.566(4)	0.043(4)	$u_3/u_1 = 1.094(50)$
d_2	Si1−F5	1.564(2)	0.043(4)	$u_2/u_1 = 0.993(50)$
d_3	Si1−O2	1.618(8)	0.047(4)	$u_3/u_2 = 1.102(55)$
d_4	O2−N3	1.478(7)	0.054(5)	$u_4/u_3 = 1.170(56)$
d_5	N3−C7	1.453(4)	0.051(5)	$u_5/u_4 = 0.962(48)$
d_6	C7−H9	1.108(7)	0.096(7)	
d_7	C7−H10	1.111(8)	0.096(8)	$u_7/u_6 = 1.005(50)$
d_8	C7−H11	1.117(8)	0.097(8)	$u_8/u_6 = 1.013(51)$
d_9	F4···F5	2.519(15)	0.070(6)	
d_{10}	F5···F6	2.627(19)	0.073(8)	$u_{10}/u_9 = 1.025(51)$
d_{11}	F4···O2	2.510(15)	0.070(6)	$u_{11}/u_9 = 1.002(50)$
d_{12}	F4···N3	3.662(12)	0.144(11)	$u_{12} = 0.149(15)$
d_{13}	F4···C7	4.550(9)	0.146(9)	$u_{13} = 0.150(15)$
d_{14}	F5···O2	2.635(14)	0.108(13)	
d_{15}	F5···N3	2.791(18)	0.176(20)	$u_{15}/u_{14} = 1.672(84)$
d_{16}	F5···C7	4.118(15)	0.183(9)	$u_{16} = 0.154(15)$
d_{17}	F5···C8	3.248(24)	0.227(11)	
d_{18}	Si1···N3	2.273(17)	0.179(16)	$u_{18} = 0.171(17)$
d_{19}	Si1···C7	3.284(11)	0.159(6)	$u_{19}/u_{17} = 0.713(36)$
d_{20}	O2···C7	2.357(7)	0.067(6)	$u_{20} = 0.074(74)$
d_{21}	C7···C8	2.439(14)	0.066(7)	$u_{21}/u_{20} = 0.989(47)$

In the gas phase, **1** adopts a Si−O−N angle [94.3(9)°], which is 17.2° larger than that in the solid state, but compares well with the MP2/6-311G(d,p) result (94.1°, Table 1). For comparison, the Si−O−N angle of the anti-conformer of $ClH_2SiONMe_2$ in the gas phase is 87.1(9)°.[20] Despite the fact that the Si···N distance of 2.273(17) Å measured for gaseous **1** is relatively large with respect to the solid-state value, there is still a considerably strong Si···N interaction. This is manifest in the distortion of the tetrahedral geometry at the Si atom, and the Si−O−N angle that is about 22° smaller than a Si−O−N angle in the hypothetical absence of Si···N attractive forces (116°).[30] The O−Si−F angles are 111.1(12)° for the out-of-(mirror)plane F atoms and 103.4(11)° for the in-plane F substituent. However, these distortions are less pronounced than in the crystal structure.

Structure in Solution. The NMR chemical shifts determined for the six different nuclei in C_6D_6 solution are listed in Table 5. C_s symmetry implies two distinct fluorine positions, which should lead to two observable ^{19}F NMR signals. The observation of one signal, even upon cooling toluene solutions of **1** to −90 °C, indicates a rapid exchange process between the different fluorine positions. MP2/6-31G(d) geometry optimizations for fixed F−Si−O−N dihedral angles were carried out to describe the rotational potential of the F_3Si group.

In Figure 4, the MP2 energy of **1** is given as a function of both the F−Si−O−N dihedral angle and the Si−O−N bending angle in the form of a three-dimensional perspective representation. The barrier to exchange of two F atoms is only 5.5 kcal mol^{-1}, which explains why we could not observe two different F signals in the NMR experiments even at −90 °C and 400 MHz proton frequency. Rotational averaging applies also for the methyl protons.

It is well-known that NMR chemical shifts of nuclei depend strongly on molecular geometry. The geometry, in turn, may depend on the environment and, therefore, NMR chemical shifts

(30) Mitzel, N. W.; Losehand, U.; Bauer, B. *Inorg. Chem.* In press.

Table 4. Correlation Matrix Elements (×100) with Absolute Values Greater than 50 for the Electron-Diffraction Least-Squares Refinement of Gaseous $F_3SiONMe_2$

$p_3\ u_1$	−83	$p_3\ u_2$	−87	$p_3\ u_3$	−81	$p_3\ u_4$	−69	$p_3\ u_5$	−62	$p_6\ p_7$	79
$p_6\ p_8$	79	$p_7\ p_8$	60	$p_9\ p_{11}$	−52	$p_9\ p_{13}$	89	$p_9\ u_{14}$	−76	$p_9\ u_{15}$	−70
$p_{10}\ p_{12}$	71	$p_{11}\ p_{17}$	51	$p_{11}\ p_{18}$	54	$p_{13}\ u_{14}$	−80	$p_{13}\ u_{15}$	−73	$p_{14}\ p_{15}$	83
$p_{14}\ p_{16}$	83	$p_{15}\ p_{16}$	69	$p_{17}\ p_{18}$	88	$p_{17}\ p_{19}$	89	$p_{18}\ p_{19}$	79	$p_{20}\ u_9$	−66
$p_{20}\ u_{10}$	−66	$p_{20}\ u_{11}$	−59	$u_1\ u_2$	86	$u_1\ u_3$	87	$u_1\ u_4$	81	$u_1\ u_5$	76
$u_2\ u_3$	88	$u_2\ u_4$	82	$u_2\ u_5$	79	$u_3\ u_4$	87	$u_3\ u_5$	80	$u_4\ u_5$	87
$u_6\ u_7$	80	$u_6\ u_8$	80	$u_7\ u_8$	63	$u_9\ u_{10}$	90	$u_9\ u_{11}$	85	$u_9\ u_{20}$	63
$u_9\ u_{21}$	56	$u_{10}\ u_{11}$	78	$u_{10}\ u_{20}$	55	$u_{11}\ u_{20}$	61	$u_{14}\ u_{15}$	91	$u_{20}\ u_{21}$	88

Table 5. Calculated and Experimental (in C_6D_6) Chemical Shift Values (in ppm) for **1** for Different Geometries Defined by the Si−O−N Angle β (in deg)[a,b]

atom no.	nucleus	$\beta = 94.1$	$\beta = 89.0$	$\beta = 84.0$	$\beta = 77.0$	$\beta_{opt} = 87.0$	Δ	exptl value
1	^{29}Si	−103.1	−108.3	−115.8	−125.6	−111.8	6.17	−117.2
2	^{17}O	131.4	136.1	142.4	159.2	138.4	1.20	137
3	^{15}N	−253.9	−260.3	−266.8	−273.7	−262.8	−13.63	−249.2
4	^{19}F	−161.5	−159.9	−156.9	−153.3	−157.9		
5,6	^{19}F	−166.9	−168.6	−169.3	−169.2	−169.3		
av(4,5,6)	$^{19}F_{av}$	−165.1	−165.7	−165.2	−163.9	−165.4	−3.57	−162.0
7,8	^{13}C	50.6	49.9	49.5	49.1	49.8	1.29	48.8
9,12	^{1}H	2.89	2.80	2.79	2.89	2.80		
10,13	^{1}H	2.38	2.37	2.39	2.44	2.38		
11,14	^{1}H	2.38	2.40	2.43	2.48	2.42		
av(all H)	$^{1}H_{av}$	2.55	2.52	2.54	2.60	2.53	0.41	2.11
all	μ^c	4.76	4.35	4.52	7.79	4.29		
all	σ^c	3.68	3.47	5.13	9.28	3.87		

[a] β_{opt} is the angle with the smallest mean absolute deviation between experimental and calculated values. The geometry of **1** was optimized for β_{opt} and NMR chemical shifts calculated for the geometry thus obtained. They differ only marginally from those obtained for β_{opt} from the curves in Figure 5a. Δ denotes the difference between calculated NMR chemical shifts for β_{opt} and the corresponding experimental data. [b] Calculated shielding values (ppm) for the following reference molecules: ^{13}C TMS 186.1, ^{29}Si TMS 351.4, ^{1}H TMS 31.18, ^{15}N $MeNO_2$ −149.9, ^{17}O H_2O 267.4, ^{19}F $CFCl_3$ (l) 180.3. These values were used to calculate NMR chemical shift values according to $\delta_X(\text{molecule}) = \sigma_X(\text{reference}) - \sigma_X(\text{molecule})$ (X denotes the nucleus) where in the case of H_2O the relationship $\sigma_{H_2O(g)} = 303.52 = \sigma_{H_2O(l)} + 36.1$ was applied and in the case of $CFCl_3$ ^{19}F chemical shifts were derived from the calculated ^{19}F shielding of HF(g) using the relationship $\sigma_{CFCl_3} = \sigma_{HF(g)} - 214.4$. [c] μ is the mean absolute deviation between experimental and calculated NMR chemical shifts and σ the corresponding standard deviation.

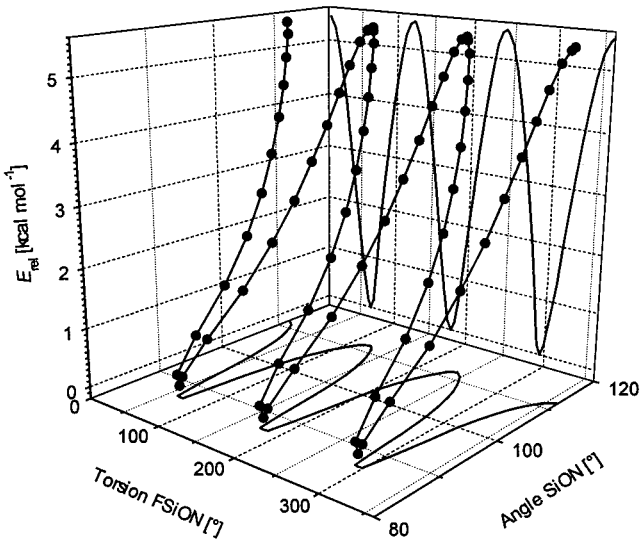

Figure 4. Three-dimensional perspective drawing of the dependence of the energy on the dihedral angle F−Si−O−N and the Si−O−N angle calculated at the MP2/6-31G(d) level of theory by complete geometry relaxation at fixed values of the dihedral angle. The one-parameter functions of the energy and angle Si−O−N are also shown as projections onto the corresponding energy-angle and torsion-angle planes.

should change in a characteristic way if a molecule is transferred from the gas to the solution phase. This is the basis of the NMR/ab initio/IGLO method[21] developed to determine molecular geometries in solution. In the case of **1**, this method was applied by calculating the geometry of **1** for six different values of the Si···N distance (Si−O−N angle), the range including both the gas-phase and the solid-state values. The NMR chemical shifts of all nuclei were then predicted for each geometry utilizing the DFT-IGLO method developed by Olsson and Cremer.[31] For comparison with the measured NMR chemical shifts, ^{19}F and ^{1}H chemical shifts were appropriately averaged to account for the rotation of the methyl and the F_3Si groups.

In Figure 5a, the deviation of the calculated shift values obtained for MP2/6-311G(d,p) geometries from the corresponding experimental shift values (zero line in Figure 5a) are given as a function of the Si−O−N angle. For an Si−O−N angle of 87.1° (Si···N distance of 2.161 Å), the smallest mean absolute deviation (4.3 ppm, Figure 5b) between measured and calculated NMR chemical shifts was obtained, which in view of typical differences of 3 (^{13}C) to 12 ppm (^{15}N) is a reasonable value.[31]

To verify the determination of the Si···N distance of **1** in C_6D_6 solution by the NMR/ab initio/IGLO method, a second set of calculations was carried out using DFT with the B3LYP functional and the large 6-311++G(3df,3pd) basis set for the calculation of the geometry of **1** at various Si···N distances (Si−O−N angles). This investigation led to a Si−O−N angle of 88.7° in reasonable agreement with the results of the first investigation. Since both MP2 and DFT provide a consistent description of the dependence of the geometry on the Si−O−N angle as the leading geometrical parameter, which is most sensitive to changes in the environment of **1**, it can be concluded that in C_6D_6 solution the gas-phase geometry changes under the impact of the surrounding benzene molecules, to a structure that is between the gas-phase structure (Si−O−N 94.3°, Figure 2) and the solid-state structure (77.1°, Figure 1). Hence, there is a continual change in geometry, electronic structure, and perhaps also bonding of **1** when transferring the molecule from

(31) (a) Olsson L.; Cremer, D. *J. Chem. Phys.* **1996**, *105*, 8995. (b) Olsson, L.; Cremer, D. *J. Phys. Chem.* **1996**, *100*, 16881.

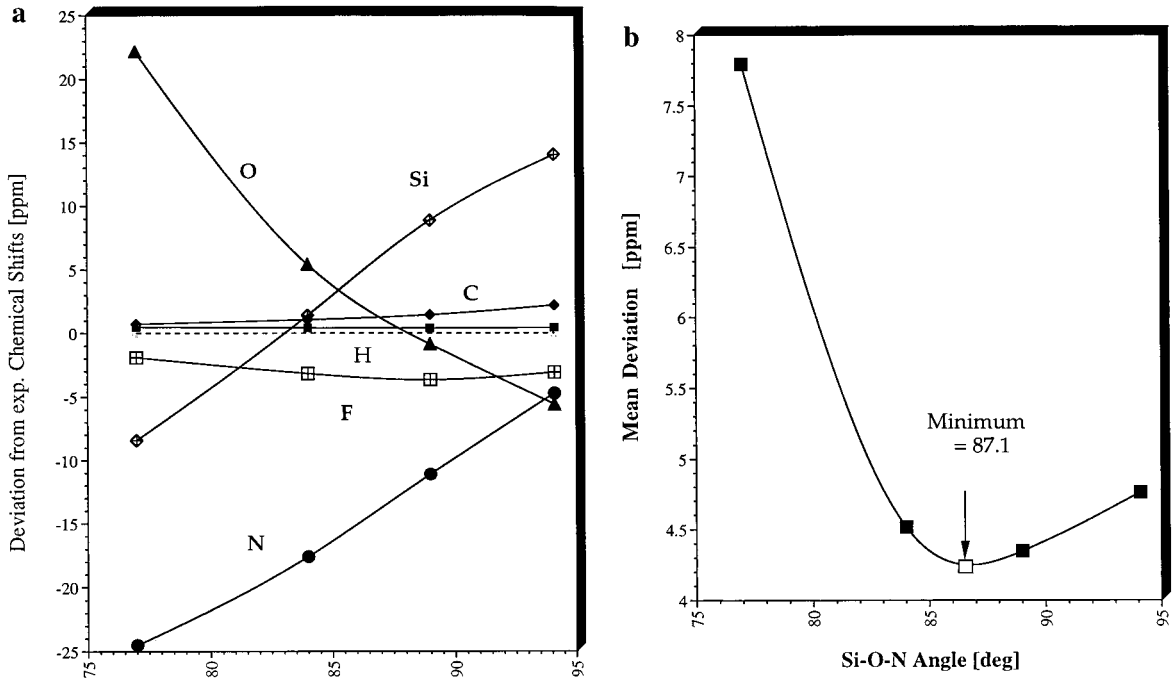

Figure 5. (a) Difference between measured (C_6D_6 solution) and DFT-IGLO ^{1}H, ^{13}C, ^{15}N, ^{17}O, ^{19}F, and ^{29}Si NMR chemical shifts of **1** as a function of the Si···N distance. All values in ppm. (b) Determination of the equilibrium value of the Si···N distance of **1** in C_6D_6 solution by NMR/ab initio/DFT-IGLO calculations. The minimum of the mean deviation of all calculated NMR chemical shifts defines the equilibrium value of the Si···N distance.

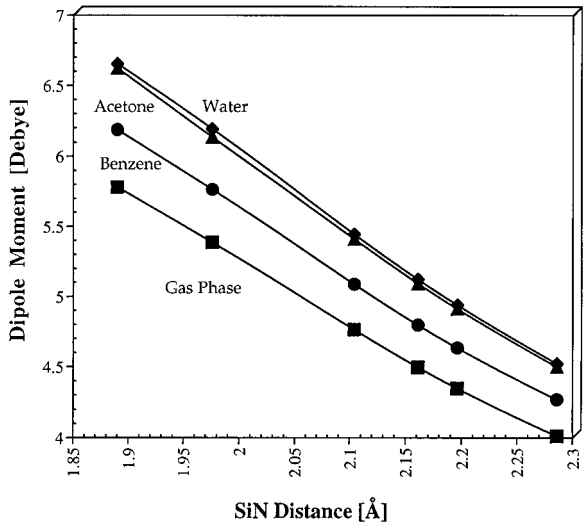

Figure 6. Calculated molecular dipole moment μ of **1** as a function of the Si···N distance and the dielectric constant ϵ [benzene, $\epsilon = 2.274$; acetone, $\epsilon = 20.7$; water, $\epsilon = 78.54$; MP2 and MP2/SCIPCM calculations with the 6-311G(d,p) basis set].

the gas to the solution phase and, finally, to the solid state. These changes will be rationalized in the following section with the help of additional quantum chemical calculations.

3. Dependence of the Electronic Nature of the SiON Linkage on the Environment

In the gas-phase molecule **1** possesses a rather large dipole moment μ of 4.0 D [MP2/6-311G(d,p) calculations], which increases considerably with shrinking Si···N distance (Si−O−N angle) as shown in Figure 6.

For an Si···N distance corresponding to the crystal structure, a dipole moment μ of 5.4 D is calculated at the MP2/6-311G-(d,p) level of theory. This can be explained by considering a vector model of the molecular dipole moment (Scheme 1). According to the electronegativity differences for Si, O, N, F, C, and H, the bond moments of a hypothetical Si−O−N-linear structure of **1** would be oriented from the Me groups to N (negative end; chemical notation), from N to O, from Si to O, and from Si to F. Because of the topology of **1**, only the Si−O bond moment is directed opposite to the other bond and group moments (Scheme 1), thus leading to maximal cancellation in the sum of group moments and to the smallest possible molecular dipole moment. When the Si−O−N unit is bent, the Si−O bond moment contributes less to the total molecular moment, which increases as shown in Figure 6.

The dipole moment of **1** is not only a suitable probe for structural changes, but also the cause for these changes. This becomes obvious when calculating the molecular geometry of **1** under the influence of a polarizable continuum, which has the same dielectric constant ϵ as benzene (2.274), the NMR solvent employed. For the geometries considered, the value of μ in benzene (4.27 to 5.77) is 0.3 to 0.4 D larger than in the gas phase ($\epsilon = 1$) as can be seen in Figure 6. This is a result of electrostatic interactions between **1** and the surrounding medium.

The molecular multipole moments (charges, dipoles, etc.) induce multipole moments with opposite charges and antiparallel orientation in the solvent and, in this way, increase stabilizing electrostatic attraction. The solvent molecules in turn increase charge separation and the molecular dipole moment of **1** by electrostatic induction, which is only possible by a contraction of the Si−O−N angle and associated changes in the geometry of **1**. These mutual interactions are largest in the solid state provided molecules **1** arrange their dipole moments in an antiparallel fashion. This is fulfilled in the lattice of the centrosymmetric space group $P2_1/n$ (Figure 1).

The changes in the molecular geometry of **1** depend on three factors. First, molecule **1** has to have a large dipole moment and structural changes must lead to a sizable change in this moment. Second, the dielectric constant of the surrounding

Scheme 1

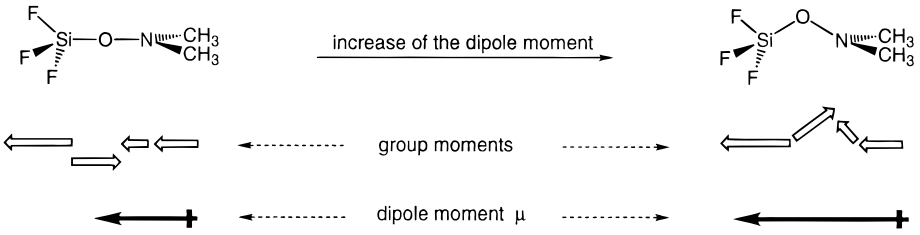

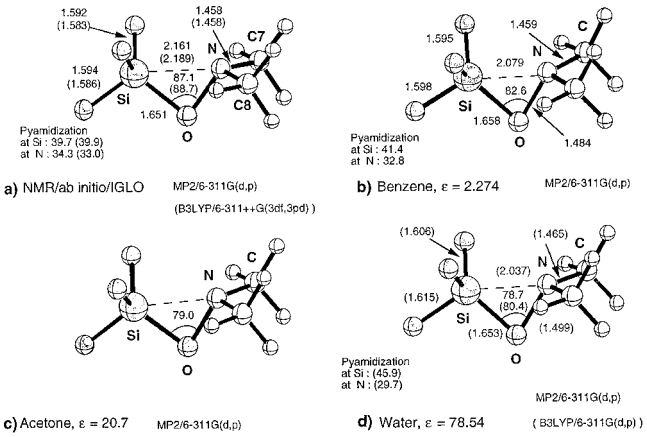

Figure 7. Geometry of **1** in solution as determined by (a) the NMR/ab initio/DFT-IGLO method using MP2/6-311G(d,p) [B3LYP/6-311++G(3df,3pd)] gas-phase geometries (see text), (b) MP2/SCIPCM/6-311G(d,p) calculations for the dielectric constant of benzene, (c) MP2/SCIPCM/6-311G(d,p) calculations for the dielectric constant of acetone, and (d) B3LYP/SCIPCM/6-311G(d,p) calculations for the dielectric constant of water.

medium must be large enough to guarantee stabilizing intermolecular interactions. Finally, the intramolecular energetic consequences of the geometry change must be such that destabilizing energy contributions are compensated by a gain of solvation or intermolecular−interaction energy.

In view of these considerations, the question arises whether the overall changes of the molecular geometry of **1** is driven by the formation of a new Si−N bond and a pentacoordinated Si atom with local trigonal bipyramidal geometry as suggested, e.g., by the crystal structure (Figure 1). We will answer this question by considering (a) the energy and geometry changes induced by the environment in more detail, (b) the energetic consequences of a new Si−N bond, and (c) the changes in the electron density distribution at Si and N.

Figure 8 illustrates the dependence of some selected geometrical parameters on the Si···N distance (ranging from the solid-state to the gas-phase value). There is a linear dependence of the Si−O−N angle on the Si···N distance [Figure 8a]. This means that either one of these parameters can be considered as the leading parameter, on which all other geometrical parameters depend. The elongation of the Si−O bond (0.031 Å) with decreasing Si−O−N angle [Figure 8b] is strongest, followed by a smaller lengthening of O−N and Si−F bonds [0.011 to 0.016 Å, Figure 8b]. At the same time the pyramidalization of the SiF_3 group [measured by the angle $\tau = 360 - \sum_{i=1,3}\alpha(FSiF)_i$] increases by 6° while pyramidalization at N decreases by 5° (Figure 8c).

The geometrical changes could be viewed as resulting from the formation of a three-membered ring with a hypervalent Si atom. To estimate the energy changes involved in the formation of a SiON ring, *N*-methyldifluorosilaoxaziridine, **2**, was investigated with the help of B3LYP/6-31G(d) calculations. The calculated geometry of **2** is shown in Figure 9 and compared with that of suitable reference molecules.

The Si−N bond length of **2** is 1.709 Å (0.25 Å shorter than in the crystal structure of **1**). The O−N bond (1.694 Å) is exceptionally long, a result of incorporating the second row atom Si with long Si−O and Si−N bonds (1.616 and 1.709 Å) into a three-membered ring, while retaining the O−Si−N angle close to 60°. Severe strain in **2** is obvious from the long O−N bond and was quantified at the B3LYP/6-31G(d) level of theory by calculation of the conventional ring strain energy (CSE) as the energy of the homodesmotic reaction 1:

$$\mathbf{2} + F_2HSi{-}OH + HO{-}NHCH_3 + F_2HSi{-}NHCH_3 \rightarrow F_2HSi{-}O{-}NHCH_3 + F_2HSi{-}N(CH_3){-}OH + HO{-}F_2Si{-}NHCH_3 \quad (1)$$

The calculated CSE is 52.7 kcal/mol, which is in line with the CSE of other three-membered rings containing both Si and O [disilaoxirane: 54.7 kcal/mol at HF/6-31G(d,p) and 47.7 kcal/mol at MP2/6-31G(d)[32]]. Since the bond energy of an Si−N bond (80 kcal mol^{-1})[33] is definitely larger than 53 kcal/mol, the energy loss due to ring strain can be compensated by the formation of a new Si−N bond. However, a Si−N bond in **1** would imply a hypervalent Si with considerably weaker bonds. Also, at 1.963 Å a Si−N bond cannot be fully established and hence the energy analysis does not provide any clue whether the assumption of (partial) Si−N bonding is justified in the case of the crystal structure of **1**.

Therefore, the electron density distribution $\rho(\mathbf{r})$ for the crystal structure of **1** and its associated Laplace concentration $-\nabla^2\rho(\mathbf{r})$[34,35] were calculated at the MP2/6-311G(d,p) level of theory and analyzed in the plane of the SiON unit [see Figure 10a,b]. No bond critical point between Si and N atom was found in the topological analysis, which is a necessary criterion for the existence of a covalent bond according to Cremer and Kraka.[36] At the midpoint between the two atoms the value of $\rho(\mathbf{r})$ is just 0.61 e/Å^3 while the Laplace concentration ($\nabla^2\rho(\mathbf{r}) = 3.1$ e/Å^5) indicates depletion of electronic charge. For comparison, the density in **2** adopts a value of 0.90 e/Å^3 at the bond critical point and 1.12 e/Å^3 at the midpoint of the Si−N bond, while the bond critical point is shifted by 20% relative to the midpoint of the Si−N bond. The electron density at the midpoint of the Si−N connection in **1** for Si−O−N = 77° is typical of a simple superposition of the densities of a Si and an N atom. Neither

(32) Cremer, D.; Gauss, J.; Kraka, E. *J. Mol. Struct. (THEOCHEM)*, **1988**, *169*, 531.
(33) Holleman, A. F.; Wiberg, E. *Lehrbuch der Anorganischen und Allgemeinen Chemie*, 100. Aufl.; De Gruyter: Berlin, 1985.
(34) (a) Bader, R. F. W. *Atoms in Molecules−A Quantum Theory*; Oxford University Press: Oxford, 1990. (b) Bader, R. F. W.; Popelier P. L. A.; Keith, T. A. *Angew. Chem.* **1994**, *106*, 647.
(35) (a) Cremer, D. In *Modelling of Structures and Properties of Molecules*; Maksic, Z. B., Ed.; Ellis Horwood: Chichester, England, 1988; p 125. (b) See ref 23. (c) See ref 35.
(36) (a) Cremer D.; Kraka, E. *Croat. Chem. Acta* **1984**, *57*, 1265. (b) Cremer D.; Kraka, E. *Angew. Chem., Int. Ed. Engl.* **1984**, *23*, 627.

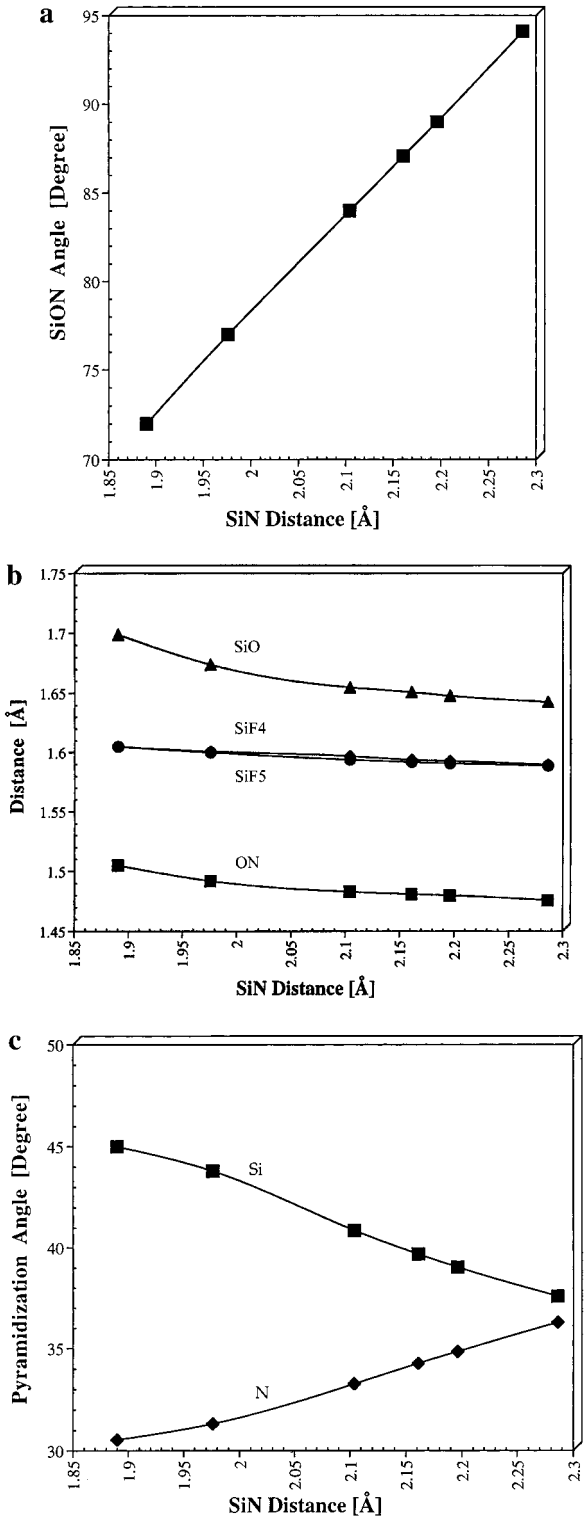

Figure 8. Dependence of geometrical parameters of **1** on the Si···N distance: (a) Si−O−N-angle; (b) Si−O, N−O, and Si−F bond lengths; and (c) pyramidalization angle at Si and N. The pyramidalization angle is defined by the expression $360 - \sum_{i=1,3}\alpha_i$, where α_i denotes the bending angles at Si or N.

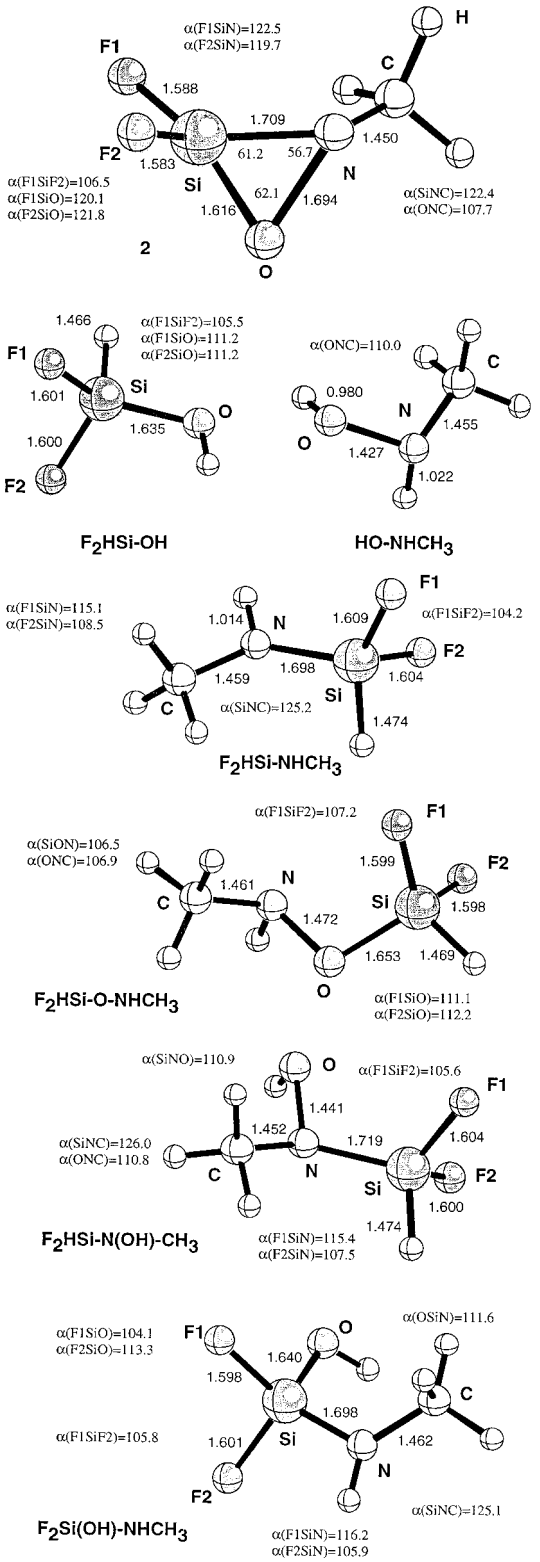

Figure 9. B3LYP/6-31G(d,p) geometries of **2** and some related reference molecules used in the homodesmotic reaction 1. Distances in Å and angles in deg.

$\rho(\mathbf{r})$ nor Laplace concentration (Figure 10a,b) provide any indication of the existence of a covalent Si−N bond in **1**.

Formation of a new Si−N bond in a polar environment would mean a D−A interaction with the N lone pair of electrons establishing the bond. Hence, the lone pair should orient along the Si−N connection line and its concentration center should be shifted toward the Si atom. Analysis of the orientation and the position of the lone pair concentration reveals that the center of the lone pair is still in the valence shell of N (distance from the N nucleus, 0.397 Å; for comparison, in **2**, the distance is 0.384 Å) and the orientation of the lone pair deviates from the Si−N connection line in the direction opposite to the O atom by 43°, i.e., it does not point toward the Si atom. We conclude that a contraction of the Si−O−N angle and the Si···N distance is not the result of covalently bonded Si···N interactions.

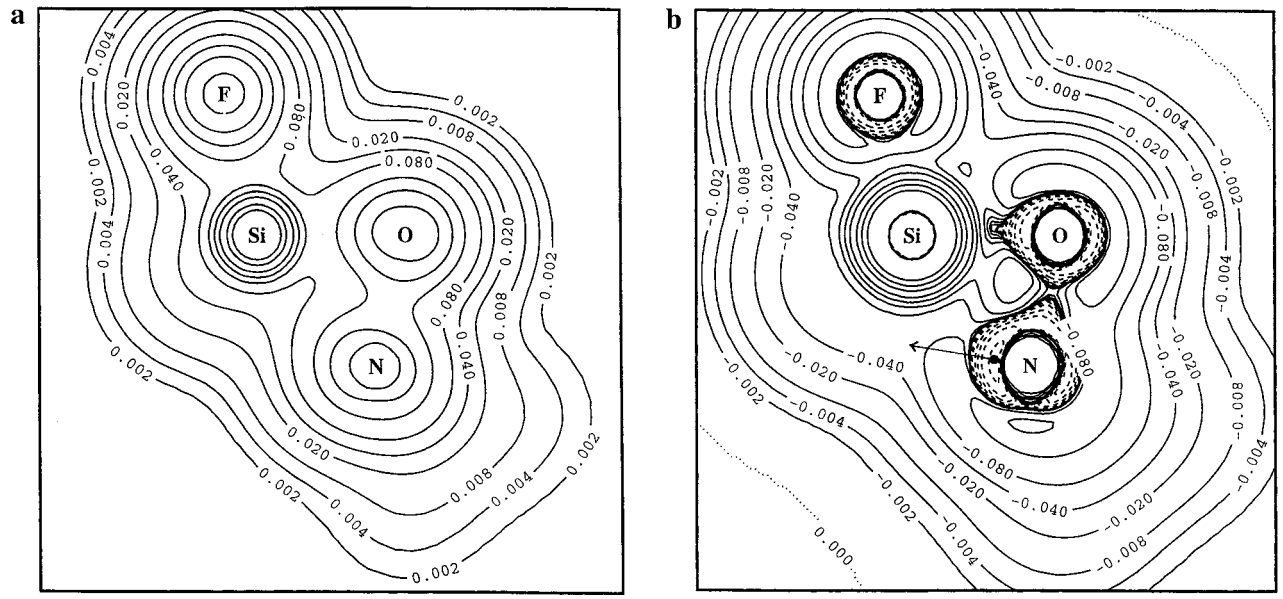

Figure 10. (a) Contour-line diagram of the electron density distribution $\rho(\mathbf{r})$ of **1** calculated for the SiON plane at a fixed Si−O−N angle of 77° using the response density determined at the MP2/6-311G(d,p) level of theory. Contour levels are given in au. (b) Contour-line diagram of the Laplace concentration $-\nabla^2\rho(\mathbf{r})$ calculated for the SiON plane at a fixed Si−O−N angle of 77° using the response density determined at the MP2/6-311G(d,p) level of theory. Solid contour levels denote charge depletion and dashed contour levels charge concentration. Contour values in au. The inner core region of the atoms is not shown. The position and orientation of the N electron lone pair are indicated.

A large change in the geometry of **1** due to electrostatic interactions is only possible if the potential energy surface (PES) of **1** in the direction of the Si−N distance is rather flat. In Figure 11, the PES of **1** is shown for four different situations, namely (a) the gas phase, (b) a benzene solution, (c) an acetone solution, and (d) an aqueous solution (the latter two are chemically noncompatible combinations in reality and serve only as hypothetical models for highly polar environments). In each of these cases the PES is rather flat. For example, changing the angle Si−O−N from its gas-phase value to its solid-state value (by 17°), the energy of an isolated molecule of **1** changes by less than 3 kcal/mol. Note that the MP2 PES is actually much flatter in the vicinity of the equilibrium than the B3LYP PES. With increasing polarity of the surrounding medium, the Si−O−N angle and the Si···N distance become smaller. The intermolecular interactions, which lead to an increase of the molecular dipole moment, are supported by stabilizing attraction between a negatively charged N atom (−0.33) and a strongly positively charged Si atom (+2.49 at Si−O−N = 77°). Since these interactions do not lead to a bond in a strained three-membered ring, energy changes remain small.

Intermolecular interactions are enhanced with increasing dielectric constant as is documented by the gain in the dipole moment (Figure 6) and the decrease of the Si−N distance: 2.062 (benzene solution, $\epsilon = 2.274$), 2.013 (acetone solution, $\epsilon = 20.7$), and 2.006 Å (water solution, $\epsilon = 78.54$), where these values were obtained by single point calculations using the gas-phase geometry. Refinement of the geometry of **1** in solution leads to the structures given in Figure 7d. Beyond a dielectric constant of 21 the changes in the molecular dipole moment (Figure 6) and the molecular geometry become marginally small.

4. Conclusions

Determination of the molecular geometry of **1** in different phases reveals an extreme dependence of the molecular structure on the surrounding medium. Compression of the Si−O−N angle by as much as 17° occurs when free molecules of **1** (gas phase) are incorporated into a crystal lattice. Accordingly, other geometrical parameters of **1** also change, although these changes are much smaller than those of the Si−O−N angle or the Si···N distance (see Figure 7). The geometrical changes are a consequence of the charge polarization in **1** and the associated large change in the molecular dipole moment, which can rise from 4 D (gas phase) to 5.5 D in benzene solution and to almost 6.5 D in acetone solution. The increase in molecular strain due to compression of the Si−O−N angle is partially compensated by electrostatic, noncovalent attraction between Si and N as is documented by a shallow PES in the direction of the Si···N distance.

It is a novel finding that the changes in the Si···N distance are not connected to the formation of a new covalent Si−N bond, but to an enhancement of noncovalent, attractive interactions between the silyl and the amino groups. As was shown for **2**, the formation of a three-membered ring would lead to an extremely large CSE (53 kcal/mol) and a marked elongation of the N−O bond. The latter is observed in the crystal structure of **1**, but to a much smaller extent than predicted for **2**. However, the analysis of the electron density distribution shows that a shortening of the Si···N distance does not lead to the formation of a covalent bond. The position of the electron lone pair at N, which would mediate a D−A bond, deviates from the N−Si connection line by more than 40°.

Results of this work are in agreement with those of related investigations on systems with donor−acceptor investigations. Using gas-phase microwave spectroscopy Ruoff and co-workers[37] observed a large dipole moment of 5.61 D for the complex SiF_4−NH_3 and argued that such a large dipole moment could only be possible if the complex is stabilized by strong electrostatic interactions rather than covalent SiN bonding. This description was confirmed by Keith and Bader,[38] who theoretically investigated atomic and molecular dipole moments by virial partitioning of the electron density distribution of the complex into atomic subspaces. They observed that the polarity

(37) Ruoff, R. S.; Emilsson, T.; Jman, A. I.; Germann, T. C.; Gutowsky, H. S. *J. Chem. Phys.* **1992**, *96*, 3441.
(38) Keith, T. A.; Bader, R. F. W. *J. Chem. Phys.* **1992**, *96*, 3447.

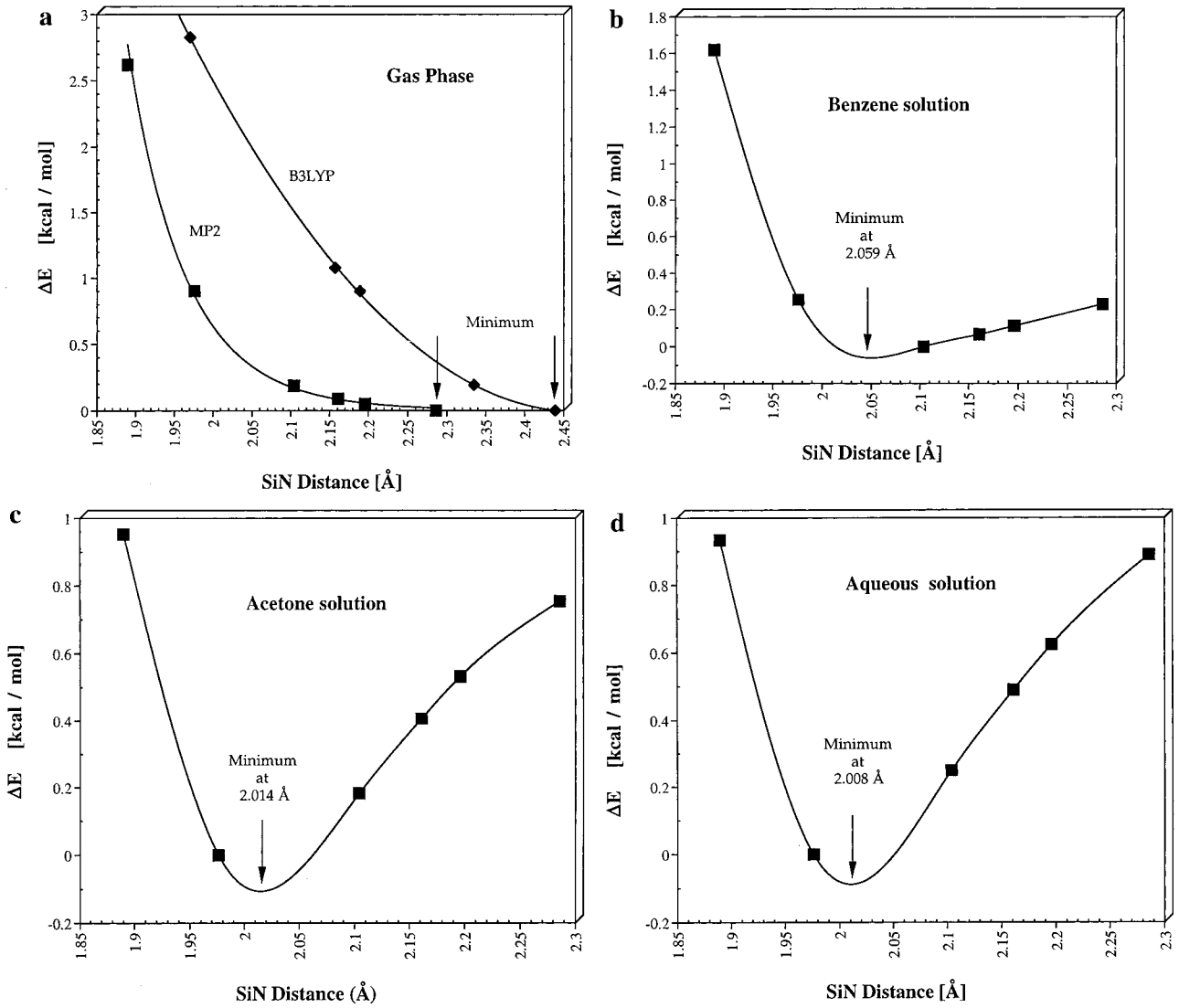

Figure 11. The potential energy surface (PES) of **1** in the direction of the Si···N distance given for (a) gas phase, (b) benzene solution, (c) acetone solution, and (d) water solution.

of the SiF bond, changes in the SiF_4 geometry upon complex formation, and strong dipole−dipole interactions between the partner molecules resulting therefrom are responsible for the complex stability. A significant transfer of charge from the N atom (donor) to the Si atom (acceptor) necessary for a covalent dative bond was not found.[38]

In recent work by Anglada and co-workers,[39] typical dative SiN interactions were theoretically investigated for a series of compounds of the type $R_nR'_{4-n}Si-NH_3$. The authors found in all cases closed shell interactions typical of electrostatic (non-covalent) attraction between Si and N. In this paper as well as in the paper about $ClH_2SiONMe_2$,[20] the widespread terminology of Haaland[3] was used to denote dative interactions as *dative bonds*, no matter whether these interactions are electrostatic or covalent in nature. Such a distinction can be done by analyzing properties of the electron density and energy density in the bonding region as demonstrated by Cremer and Kraka;[35] it will become however problematic if just Mulliken or NBO charges or the Laplacian of the electron density distribution are used since clear definitions of covalent or electrostatic interactions based on these quantities are not known (the Laplacian becomes positive for the F−F bond thus failing the covalent character of this bond).[36]

Molecule **1** differs from most other D−A complexes with strong variations in the D−A bond length upon changes in the environment insofar as the D and the A groups belong to the same molecule (as is also the case for silatranes) and do not imply a change in bonding. To the best of our knowledge, the geometrical changes observed for **1** are the largest for a nonbonding interaction between geminal substituents (amino and silyl) of an ether. They are dipole moment driven, which makes **1** and related compounds candidates for molecular devices that change their geometry upon changes in a surrounding electrical field. The results obtained in this work suggest that other D−X−A molecules with intramolecular D−A interactions should be (re)investigated, in view of the nature of the D−A interactions, which were often assumed to be covalent, but may be predominantly electrostatic as in the case of **1**.

5. Experimental and Quantum Chemical Details

General. The experiments were carried out using a standard Schlenk line or in a vacuum line with greaseless stopcocks (Youngs taps), which was directly attached to the gas cell in an FTIR spectrometer (Midac Prospect FTIR). *N,N*-Dimethylhydroxylamine was liberated from its hydrochloride with liquid NH_3. Me_2O was dried over CaH_2. All NMR

(39) Anglada, J. M.; Bo, C.; Bofill, J. M.; Crehuet, R.; Poblet, J. M. *Organometallics* **1999**, *18*, 5584.

spectra were recorded at 21 °C on a JEOL JNM-LA400 spectrometer in sealed tubes with C_6D_6 as a solvent directly condensed onto the sample from K/Na alloy. NMR references: ^{1}H, ^{13}C, and ^{29}Si TMS, ^{15}N $MeNO_2$, ^{17}O H_2O, and ^{19}F $CClF_3$.

(*N,N*-Dimethylaminoxy)trifluorosilane. $HONMe_2$ (1.1 mL, 0.9 g, 15 mmol) was dissolved in pentane (20 mL), treated with an *n*-BuLi solution (1.8 M in hexane, 0.83 mL) at −50 °C, and allowed to warm to ambient temperature. After removal of the solvents in a vacuum a residue of 0.8 g of $LiONMe_2$ (12 mmol) remained, onto which dimethyl ether (30 mL) and SiF_4 (1.2 g, 12 mmol) were condensed at −196 °C. The mixture was stirred for 6 h at −96 °C and consequently fractionated through a series of cold traps held at −25, −96, and −196 °C, with the crude product (0.6 g) retained in the −96 °C trap. This colorless liquid was again fractionated through traps held at −35, −40, −96, and −196 °C, whereby pure $F_3SiONMe_2$ was collected in the −96 °C trap, while small amounts of $F_2Si(ONMe_2)_2$ were stopped in the −35 and −40 °C traps. ^{1}H NMR δ 2.10 (q, $^5J_{HCNOSiF}$ = 0.7 Hz, 6H, H_3C). ^{13}C NMR δ 48.8 (q q, $^1J_{CH}$ = 138.1 Hz, $^3J_{CNCH}$ = 4.8 Hz, CH_3). ^{15}N-{^{1}H} NMR δ −249.2 (q, J_{NF} = 9.3 Hz). ^{17}O{^{1}H} NMR δ 137 (s). ^{19}F NMR δ −162.0 (s). ^{29}Si NMR δ −117.2 (q, $^1J_{SiF}$ = 179.2 Hz). IR-(Gas) υ [cm^{-1}]1035 (s, νSiF), 1030 (s, δSiF), 990 (s, νSiF).

Crystal Structure Determination of $F_3SiONMe_2$. A single crystal of $F_3SiONMe_2$ was grown in situ by slowly cooling the melt in a sealed capillary below the melting point of −64 °C after generation of a suitable seed crystal by shock freezing and microscale zone refinement slightly below the melting point. $C_2H_6F_3NOSi$: M_r = 145.17, crystal system monoclinic, space group $P2_1/n$, Z = 4, a = 5.8709(8) Å, b = 9.8771(8) Å, c = 10.491(3) Å, β = 104.408(7)°, V = 589.2(2) Å^3 at 133(2) K, μ = 0.369 mm^{-1}, $2\theta_{max}$ = 80.14°, ω-scan, 3635 independent reflections [R_{int} = 0.047], 97 parameters, R_1 = 0.0466 for 2373 reflections with $F_o > 4\sigma(F_o)$ and wR_2 = 0.1382 for all 3635 data. Solution by direct methods and refinement of the structure were undertaken with the program SHELXTL 5.01.[40]

Gas-Phase Electron Diffraction. Electron scattering intensity data for **1** were recorded on Kodak Electron Image plates using the Edinburgh electron diffraction apparatus and a wavelength of 0.06016 Å.[41] The samples were held at −60 °C and the inlet nozzle at 20 °C during the experiments. Scattering data for benzene were recorded concurrently and used to calibrate the electron wavelength and camera distances. Three exposures were taken at each camera distance (285.38 and 128.21 mm). Data in the ranges s = 2.0−13.8 and 6.0−32.8 Å^{-1} were obtained in digital form using the microdensitometer at the Institute of Astronomy at Cambridge.[42] The data analysis followed standard procedures, using established data reduction and least-squares refinement programs[43] and the scattering factors established by Fink and co-workers.[44] The weighting scheme for the applied trapezoidal weighting functions was s = 4.0 and 11.8 Å^{-1} for the long camera distance and 8.0 and 28.0 Å^{-1} for the short camera distance, the correlation parameters 0.4769 and 0.4065, and the refined scale factors 0.693(5) and 0.695(5). The refined molecular parameters, their definitions and the applied restraints, a list of selected interatomic distances including vibrational amplitudes and applied restraints, and elements of the correlation matrix are given in Tables 2−4. The final R factors for long and short camera distance data sets were 0.042 and 0.046, the overall R_g value 0.044.

Quantum Chemical Calculations. Geometry optimizations and vibrational frequency calculations were performed with analytic first- and second-derivatives at the Hartree−Fock (HF), MP2, and DFT levels of theory. Different basis sets of increasing size were employed, namely the standard basis sets 3-21G(d), 6-31G(d), and 6-31G(d,p) as well as the more extended 6-311G(d,p), 6-311+G(d,p), and 6-311++G(3df,-3pd) basis sets.[45] All MP2 calculations were carried out with a frozen core. For the DFT calculations the B3LYP exchange-correlation functional was used.[46]

Sum-over-states density functional perturbation theory (SOS-DFPT)[47] based on the "individual gauge for localized orbitals" (IGLO)[48] was employed to calculate NMR chemical shieldings for **1**.[31] At the DFT level, a combination of the Becke exchange[49] and the PW91 correlation functionals[50] rather than B3LYP was used since the former leads to somewhat better shift values.[31] The (9s5p1d/5s1p) [5s4p1d/3s1p] basis set was employed (VTZ+P quality)[51] for IGLO calculations. All DFT calculations were based on an accurate calculation of the Coulomb part and numerical integration of the exchange-correlation potential. The well-known deficiencies of DFT methods lead to occupied orbitals with relatively high energies and to an overestimation of paramagnetic contributions to chemical shifts,[47] for which compensation was made by adding appropriate shift factors to orbital energy differences.[31] The NMR/ab initio/IGLO method for investigating the geometry of **1** in C_6D_6 solution was applied in the manner described in the literature.[21]

The energy and geometry of **1** in solution were determined by using a reaction field with the self-consistent isodensity polarized continuum (SCIPCM) approach,[52] a simplified form to mimic electrostatic solvent effects. In this approach, an isodensity surface defined by a value of 0.0004 au of the total electron density distribution is calculated at the level of theory employed. Such an isodensity surface has been found to define rather accurately the volume of a molecule[53] and, therefore, it should also define a reasonable cavity for the dissolved molecule within the polarizable continuum where the cavity can iteratively be adjusted when improving wave function and electron density distribution during a self-consistent field (SCF) calculation at the MP2 or DFT level. The IPCM method has the advantage that geometry optimization of the solute molecule can be carried out at the level of theory chosen for the description.

Two different ways of determining the impact of the solvent on the solute were pursued. First, MP2/SCIPCM or DFT/SCIPCM energies for the dielectric constant ϵ of benzene (2.274 at 25 °C),[54] acetone (20.7),[54] and water (78.54)[54] were determined by utilizing MP2 or DFT geometries of **1** obtained for fixed values of the Si−O−N angle in the gas phase. In this way, the PES curves of Figure 11 were obtained. The estimated values of Si−N distance (Si−O−N angle) were then used to define the starting geometry for a complete geometry optimization at the given value of the dielectric constant ϵ.

The electron density distribution $\rho(\mathbf{r})$, in the form of either an expectation property (DFT) or a response density (MP2),[55] was analyzed using the virial partitioning method of Bader and co-workers.[33] The covalent character of a given bond was classified by application of the criteria given by Cremer and Kraka.[35] The Laplace concentration $-\nabla^2\rho(\mathbf{r})$ was analyzed to determine regions of charge concentration and depletion. The position of the N lone pair was calculated as that of the

(40) SHELXTL 5.01, Siemens Analytical X-ray Instrumentation Inc.: Madison, WI, 1995.

(41) Huntley, C. M.; Laurenson, G. S.; Rankin, D. W. H. *J. Chem. Soc., Dalton Trans.* **1980**, 945.

(42) Lewis, J. R.; Brain, P. T.; Rankin, D. W. H. *Spectrum* **1997**, *15*, 7.

(43) Mitzel, N. W.; Brain, P. T.; Rankin, D. W. H. *ED96*, Version 2.0, 1998. A program for gas-phase electron-diffraction structure refinement developed on the basis of formerly described ED programs: Boyd, A. S. F.; Laurenson G.; Rankin, D. W. H. *J. Mol. Struct.* **1981**, *71*, 217.

(44) Ross, A. W.; Fink M.; Hilderbrandt, R. *International Tables for X-ray Crystallography*; Wilson, A. J. C., Ed.; Kluwer Academic Publishers: Dodrecht, Boston, 1992; Vol. C, p 245.

(45) (a) Binkley, J. S.; Pople, J. A.; Hehre, W. J. *J. Am. Chem. Soc.* **1980**, *102*, 939. (b) Gordon, M. S.; Binkley, J. S.; Pople, J. A.; Pietro, W. J.; Hehre W. J. *J. Am. Chem. Soc.* **1982**, *104*, 2797. (c) Pietro, W. J.; Francl, M. M.; Hehre, W. J.; Defrees, D. J.; Pople, J. A.; Binkley J. S. *J. Am. Chem. Soc*. **1982**, *104*, 5039. (d) 6-31G(d): Hariharan, P. C.; Pople J. A. *Theor. Chim. Acta* **1973**, *28*, 213. (e) Hariharan, P. C.; Pople, J. A. *Chem. Phys. Lett.* **1972**, *66*, 217. (f) 6-311G(d): Krishnan, R.; Frisch, M. J.; Pople, J. A. *Chem. Phys.* **1980**, *72*, 4244.

(46) (a) Becke, A. D. *J. Chem. Phys.* **1993**, *98*, 5648. (b) Stephens, P. J.; Devlin, F. J.; Chablowski C. F.; Frisch, M. J. *J. Phys. Chem.* **1994**, *98*, 11623.

(47) Malkin, V. G.; Malkina, O. L.; Salahub, D. R. *Chem. Phys. Lett.* **1993**, *204*, 80.

(48) Schindler, M.; Kutzelnigg, W. *J. Chem. Phys.* **1982**, *76*, 1919.

(49) Becke, A. D. *Phys. Rev. A* **1988**, *38*, 3098.

(50) Perdew, J. P.; Wang, Y. *Phys. Rev. B* **1992**, *45*, 13244.

(51) Kutzelnigg, W.; Fleischer, U.; Schindler M. In *NMR, Basic Principle and Progress*; Diehl, P., Ed.; Springer: Berlin, 1991; Vol. 23, p 165.

(52) Foresman, J. B.; Keith, T. A.; Wiberg, K. B.; Snoonian, J.; Frisch, M. J. *J. Phys. Chem.* **1996**, *100*, 16098.

(53) Gough, K. M. *J. Chem. Phys.* **1989**, *91*, 2424.

(54) *Handbook of Chemistry and Physics*, 72 ed.;, Lide, D. R., Ed.; CRC Press: Boca Raton, 1991.

(55) Kraka, E.; Gauss, J.; Cremer, D. *J. Mol. Struct. (THEOCHEM)* **1991**, *234*, 95.

concentration maximum in the nonbonding region of N.[24] Atomic charges were calculated using the natural atomic orbital (NAO) population analysis.[56] All calculations were performed with the ab initio programs COLOGNE 99[57] and GAUSSIAN 98.[58]

Acknowledgment. This work was supported by the Bayerisches Staatsministerium für Wissenschaft, Forschung und Kunst (Bayerischer Habilitationsförderpreis 1996 for N.W.M.), the Deutsche Forschungsgemeinschaft (grant MI477/3-3), the Fonds der Chemischen Industrie, the Leonhard-Lorenz-Stiftung, the Swedish Natural Science Research Council (NFR) in Göteborg, and the EPSRC (grant GR/K44411). Bayer AG is thanked for a donation of *N*,*N*-dimethylhydroxylamine hydrochloride. The calculations were performed on the Cray-C94 computer of the Nationellt Superdatorcentrum (NSC), Linköping, Sweden, and the VPP at the Leibniz-Rechenzentrum, München. D.C. thanks the NSC for a generous allotment of computer time. N.W.M. and U.L. are grateful to Prof. H. Schmidbaur (Garching) for generous support of this work.

Supporting Information Available: Tables of crystal and structure refinement data, atomic coordinates, bond lengths and angles, anisotropic displacement parameters, and hydrogen coordinates for $F_3SiONMe_2$ (PDF). This material is available free of charge via the Internet at http://pubs.acs.org.

JA994542W

(56) (a) Carpenter J. E.; Weinhold, F. *J. Mol. Struct. (THEOCHEM)* **1988**, *169*, 41. (b) Reed, A. E.; Weinhold, F. *J. Chem. Phys.* **1983**, *78*, 4066. (c) Reed, A. E.; Curtiss, L. A.; Weinhold, F. *Chem. Rev.* **1988**, *88*, 899.

(57) COLOGNE 99, Kraka. E.; Gräfenstein, J.; Gauss, J.; Reichel, F.; Olsson, L.; Konkoli, Z.; He, Z.; Cremer, D.; Göteborg University, Sweden, 1999.

(58) Gaussian 98, Revision A.6, Frisch, M. J.; Trucks, G. W.; Schlegel, H. B.; Scuseria, G. E.; Robb, M. A.; Cheeseman, J. R.; Zakrzewski, V. G.; Montgomery, J. A., Jr.; Stratmann, R. E.; Burant, J. C.; Dapprich, S.; Millam, J. M.; Daniels, A. D.; Kudin, K. N.; Strain, M. C.; Farkas, O.; Tomasi, J.; Barone, V.; Cossi, M.; Cammi, R.; Mennucci, B.; Pomelli, C.; Adamo, C.; Clifford, S.; Ochterski, J.; Petersson, G. A.; Ayala, P. Y.; Cui, Q.; Morokuma, K.; Malick, D. K.; Rabuck, A. D.; Raghavachari, K.; Foresman, J. B.; Cioslowski, J.; Ortiz, J. V.; Stefanov, B. B.; Liu, G.; Liashenko, A.; Piskorz, P.; Komaromi, I.; Gomperts, R.; Martin, R. L.; Fox, D. J.; Keith, T.; Al-Laham, M. A.; Peng, C. Y.; Nanayakkara, A.; Gonzalez, C.; Challacombe, M.; Gill, P. M. W.; Johnson, B.; Chen, W.; Wong, M. W.; Andres, L. J.; Gonzalez, C.; Head-Gordon, M.; Replogle, E. S.; Pople, J. A. Gaussian, Inc.: Pittsburgh, PA, 1998.